The Fourth IEEE RAS/EMBS International Conference
on Biomedical Robotics and Biomechatronics
Roma, Italy. June 24-27, 2012

An Actuated Phantom for Developing and Studying MRI-Guided Interventions in Dynamic Environments

Nicholas C. von Sternberg, Yousef S. Hedayati, Habib M. Zaid, Erol Yeniaras,
Eftychios Christoforou, and Nikolaos V. Tsekos

Abstract— **During early development stages of novel medical technologies the use of cost-effective, reusable and adaptable dynamic models can be an effective precursor to animal studies. This paper describes and demonstrates a novel, MR compatible, actuated phantom which can mimic the global motion of the left ventricular corridor. This prototype has five actuated DoF and is controlled to replicate specific in vivo motion according to pre-collected MR images. Studies conducted demonstrate 21.1% open-loop error in replicating 1.57 mm motions. MR studies in a 1.5T clinical scanner manifested that the system is MR compatible. SNR was measured to be 90.9 ± 15.4 with the motors in motion and 89.4 ± 2.6 with the motors idle. The purpose of this device is to be used as a phantom for the development and validation of image-guided and robot-assisted intracardiac surgeries in the beating heart.**

I. Introduction

The emergence of minimally invasive surgeries (MIS) and image-guided interventions (IGI) has primed innovative research of new procedures which could highly impact the future of healthcare via improved patient treatment and cost effectiveness. This paradigm shift entails the systematic improvement of current approaches, as well as the development of new approaches, for real-time sensing and the control of dexterous robotic manipulators (e.g. [1-3] and references therein). The development of enabling methodologies and technologies to perform MIS within dynamic environments, such as the free beating heart, is challenging because natural motion continuously alters the Area of Operation (AoO).

The development, validation and optimization of new clinical approaches require in vivo studies on animal models and eventually on humans. Whereas animal and human studies are absolutely necessary for eventual acceptance of any new method, development of these procedures would benefit greatly from validation on a phantom before testing on living models. Phantoms that can mimic the physical properties, dimensions, and motion of the tissue of interest can provide an accurate and reusable representation of the dynamic environment to validate and optimize the procedure. Several such phantoms, including anthropomorphic ones, are used in both surgical research and in training [4, 5].

Magnetic resonance imaging (MRI) has emerged as a promising guidance modality since (1) it offers a plethora of contrast mechanisms for assessing morphology and function, (2) protocols exist for visualizing interventional tools and robotic manipulators, (3) it is true three-dimensional (3D) and multislice, and (4) its operation does not require any ionizing radiation. MR-guided robot-assisted interventions have evolved significantly [6] and recently MR guidance has been demonstrated in transapical aortic valve interventions [5, 7]. Further development of such image-guided surgeries requires extensive experimentation to account for the complex and dynamic environment in vivo [8-10].

Towards addressing this need, the goal of this work was to design an MR compatible, computer controlled, and actuated phantom that can mimic the motion of tubular structures. An initial example of such a tubular structure is the left ventricular access corridor (LVAC) which is an important cardiac landmark for robot-assisted transapical intracardiac surgeries of the beating heart. In addition to being part of the ongoing development of a system for image-guided intracardiac surgeries [8-10], the primary motivations for developing such a device are the following:

- Reduce the development cost for imaging and robotic systems, as compared to animal or excised heart models.
- Reduce the number of animal studies; relieving some of the pressure by the ethical dilemmas of animal testing.
- Serve as a versatile and reusable test bed for evaluating the methods of procedure practice, and as a training platform.

In our previous work [11] we describe the theoretical design of such a phantom. This paper describes the first version of an MR compatible prototype of a dynamic phantom, with 5 degrees-of-freedom (DoF) for mimicking the global motion of the LVAC or other tubular structures in the heart. Also presented in this work are experimental studies assessing the mechanical accuracy and the MR compatibility of the phantom inside of a 1.5T clinical scanner.

This work was supported by the National Science Foundation under Grant CNS-0932272. All opinions, findings, conclusions or recommendations expressed in this work are those of the authors and do not necessarily reflect the views of our sponsors.

NCvS, YSH, and HMZ are with the Medical Robotics Lab, Department of Computer Science, University of Houston, Houston, TX, USA (E-mail: nvonsternberg, yshedayati, hmzaid @uh.edu)

EY is with the University of Texas MD Anderson Cancer Center, Houston, TX, USA (E-mail: eyeniaras@mdanderson.org)

EC is with the KIOS Research Center at the University of Cyprus, Nicosia, Cyprus (E-mail: e.christoforou@ucy.ac.cy)

NVT is with the Medical Robotics Laboratory, at the Department of Computer Science, at the University of Houston, Houston, TX 77204 USA (Phone: 713-743-3350; Fax: 713-743-333; E-mail: ntsekos@cs.uh.edu)

II. METHODS

A. Concept for Motion Replication

Fig. 1 illustrates the topography of the human heart showing a long-axis MR image together with a virtual flexible robotic manipulator (blue) that enters via a transapical trocar (pink) and advances through the LVAC to the aortic annulus for delivering a prosthetic aortic valve [8]. Analysis of this topography reveals the critical landmarks of the heart associated with such a procedure. Such landmarks include: the apex (through which a trocar is inserted), the endocardial surface of the LVAC, and the aortic annulus. As shown in Fig. 1, a simple, yet accurate way to represent those landmarks would be with tubular structures.

In the free beating heart, secondary to its motion, those landmarks and the associated mimicking tubular structures, move continuously. If the dimensions and motion of these landmarks are extracted and an appropriate kinematic structure is created, then their combined motion, relative position, and size can mimic the moving AoO. To demonstrate this concept we have first designed a phantom which consists of an actuated tube to mimic the LVAC.

To validate a robot-assisted valve implantation, Li et. Al [5] used a plastic tube in a water tank to simulate an aortic annulus. While experiments with this static phantom validated basic control and MRI compatibility, a fixed tubular structure is not suitable for evaluating a robot's ability to account for the motion of the beating heart. An actuated tubular structure would provide a more realistic replication of the AoO and, through resulting validation, may reduce the number of animal studies.

In practice, all three-dimensional (3D) motion of the anatomical structure except rotation around the Z axis, can be represented by the Cartesian coordinates: X, Y, Z, of the two centers P1 and P2 (Fig. 1). The open faces of the tubular structure, P1 and P2, move independently as the heart beats and can be actuated by two separate Cartesian stages.

B. MR-Compatibility by Remote Actuation

While several types of actuators can be used for MR compatibility including pneumatic, piezoelectric and hydraulic [5, 6, 12], we have selected standard electromagnetic stepper motors in this work to reduce the cost as well as the complexity of implementation and control.

Since electromagnetic stepper motors are not MRI compatible *per se* we implemented a system to locate them at a safe distance away from the scanner's magnetic center. This distance is based specifically on the fringe field of the scanner used in this study, which is the Siemens MAGNETOM Avanto 1.5T MR scanner. The static fringe field strength provided by the manufacturer's planning guide, shown in Fig. 2 as a contour plot, lead us to believe that the field strength experienced in the range of 2 to 2.5 meters (m) from the center of the scanner the field is approximately between 20 and 5 milliTesla (mT) respectively. For reference, common refrigerator magnets are approximately 5 mT. Therefore it was decided that a phantom 2.5 m in length would allow the end-effectors to be brought into the bore of the machine while the motors remain in a region of low magnetic field.

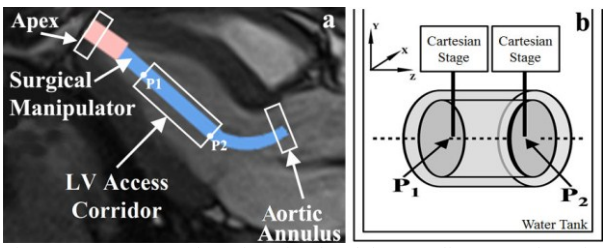

Fig. 1. a) Topography of a simulated intracardiac procedure for aortic valve annuloplasty using a robotic manipulator. Relevant cardiac landmarks: apex, left ventricular (LV) access corridor and aortic annulus superimposed to long axis image of the heart. b) Tracking points P1 and P2 of the LV access corridor.

C. Design of Remote Actuation

Specifically, actuation (Fig. 3) is transferred to the point of interest via two Cartesian stages (a) and (b) capable of actuating a tubular structure (c) by changing the position of the remote points (d) and (e) along the three Cartesian directions X, Y, and Z.

The Cartesian stage (Fig. 4) is composed of a 2.5 m rolling platform (a) which extends from the motor side (b) of the stage to the actuation side (c). This platform rolls on the phantom base to give motion along the Z axis (long axis of the MRI). On top of this platform rest two carts which are actuated by the same driveshaft so that their movement is coupled. One cart (d) contains a motor and the other cart (e) contains a rack and pinion. The parallel movement of these carts provides movement of the end-effector in the X direction (horizontal short axis), while the motor and rack and pinion mechanism inside of the carts actuate the end-effector in the Y direction (vertical long axis). The color scheme of Fig 4 represents the direction of movement for each part. Parts which move in the X, Y, and Z directions are colored red, yellow, and green respectively. Motion of both Cartesian stages provides resulting 3D positioning to the anatomical structure (f).

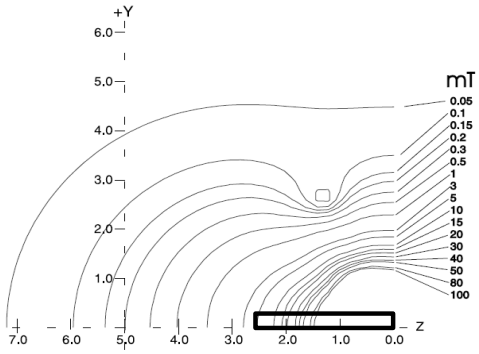

Fig. 2. Fringe field for the Siemens MAGNETOM Avanto 1.5T MR Scanner. Origin at the magnetic center. Axis units are meters. Box represents the area which the phantom will occupy.

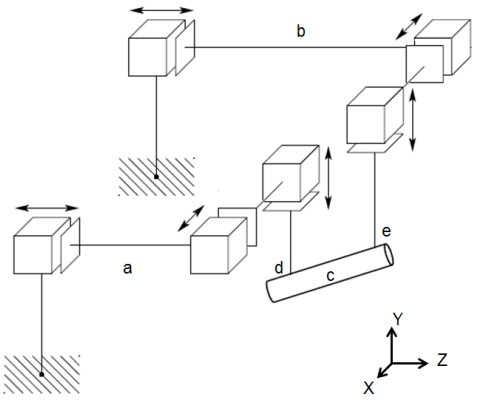

Fig. 3. Kinematic diagram of two Cartesian stages (a) and (b) used to actuate one tubular structure (c) by changing the 3D position of the two points (d) and (e).

D. Physical Prototyping

In addition to the remote placement of the actuators, to ensure MR-compatibility and safety in physical prototyping, non-paramagnetic materials were selected for placement inside of the MRI scanner. Non-conductive materials were preferred because they will not produce imaging artifacts. Acknowledging these constraints the phantom is constructed mostly of plastic and composite materials such as ABS, acrylic, carbon fiber, and fiberglass. Non-magnetic metals were used sparingly where necessary. These items include aluminum rivets used to fasten the vertical pillars along the frame of the phantom and brass spur racks and gears used to transfer motion on the carts (d) and (e) of Fig 3.

E. Motion Replication

To drive the motion of the tubular structure that represents the LVAC the control software and hardware provides the appropriate modules for MR-based or user-defined motion trajectories. To mimic the motion of those landmarks based on actual *in vivo* data, we extracted the motion of corresponding landmarks from MRI CINE images, with the process described in [8]. The motion data is derived from sets of CINE images collected from healthy volunteers. The datasets included nineteen short and five long axes slices depicting 25 frames for each heart cycle. Blood pooling in images was segmented to find the LV structure Sc(t) (Fig. 5). From the structure Sc(t) points P1 and P2 (Figs. 1 and 3) were defined for the left ventricular corridor. This data is used to define the motor trajectory.

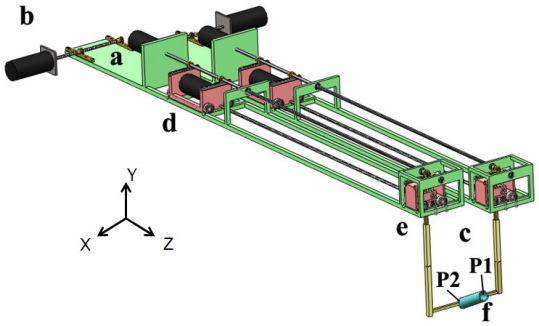

Fig.4. Basic model of the actuation mechanism. a) Z platform, b) Motor side, c) Actuation side, d) Motor cart, e) Rack and pinion cart f) Anatomical structure. Color indicates direction of movement. This model is not drawn to scale.

F. Motion Control

Actuation of the phantom consists of accurately positioning the tubular structure representing the LVAC. Each end of the tube is positioned using relative coordinates derived from the MR CINE data. The tube is actuated from two opposing sides creating the need for two independent Cartesian stages. Each stage uses three motors, one for each Cartesian direction, requiring six motors in total. Due to the size constraints, the motors used in this design are NEMA 11 hybrid stepper motors for the X and Y directions, and NEMA 23 stepper motors for the Z direction. Each motor is paired with a rotary optical encoder (Anaheim Automation, Anaheim, CA).

Each tube is linked to the stage via universal joints. This configuration allows the tube to translate in X, Y, and Z directions and rotate about the X axis and Y axis but not the Z axis. This configuration therefore provides five output degrees of freedom (DoF) resulting from six input DoF.

Currently many devices are using active and passive fiducial tracking for positioning within an MRI scanner [6, 13] and references therein. However, with appropriate calibration, the optical encoders of the motors can provide position feedback without requiring additional data from the MRI scanner [12, 14]. This will allow the aforementioned tracking systems to be implemented on the devices of which the phantom is designed to test, bypassing additional imaging demands for the control needs of the phantom.

Gecko 251 stepper drivers (Geckodrive, USA) are used to actuate the motors. These drivers feature fixed 10X microstepping which increases the motor precision from 200 to 2000 steps per rotation. The drivers accept step and direction command inputs and output necessary current to the motor to adjust the position accordingly. Step and direction signals are the output of a closed-loop position control scheme implemented on an Altera DE2-115 Field

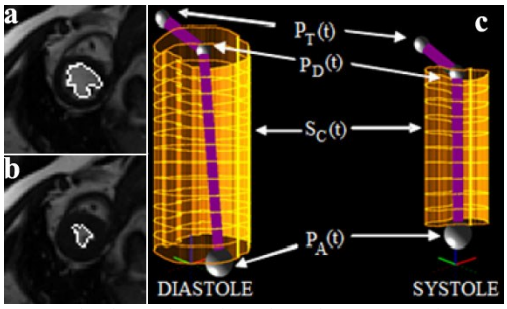

Fig. 5. Derivation of motion data from CINE images using segmentation of blood pooling in the LV. a) Short axis diastole, b) short axis systole, c) Resulting structure Sc(t). Points $P_T(t)$, $P_D(t)$, and $P_A(t)$ represent points along a simulated surgical end effector.

Programmable Gate Array (FPGA) (TerasIC, Taiwan). This FPGA was used in place of the multiple microcontrollers proposed in our previous work [11] because it can be programmed to perform control calculations and decode quadrature encoders for all motors in parallel on a single device. The actuated phantom can mimic operator defined motions, as well as replicate the motion of the heart extracted from cardiac dynamic imaging. In those studies, we investigated the actuated phantom with the motion pattern of the human beating heart extracted from CINE MRI data of healthy volunteers. Datasets containing 25 points were extracted for each one of 6 points to be actuated. To simulate a heart cycle at 60 beats per minute, these 25 points are repeated at even intervals over 1 second.

G. *Bench-top Experimental Studies*

To test the response of the system, the device's movement was tested with only open loop movements. The individual two stages were given equivalent movement commands and their positions were tracked using a 10-camera motion capture system (VICON, USA) as described in [15]. Fig. 6(a) shows the phantom in the motion capture setup and the two sensors attached for tracking the motion can be seen in Fig. 6(b). These two points are analogous to the points P1 and P2 as seen in Figs. 1 and 3. By tracking these two points, the orientation of the tube representing the LVAC can be determined. For this setup the imaging modality is an optical motion capture system, but a similar configuration can be easily implemented for MRI as well.

III. RESULTS

A. *Heart Motion Data Extraction*

Three main constraints in the design of this phantom were: dimensional accuracy to that of a human heart, limited space inside the bore of the MRI scanner, and proper material selection to ensure both safety and image integrity. In order to design a phantom that accurately depicts the dimensions of a human heart, MRI CINE data was taken from ten healthy volunteers. Analysis of this data determined the maximum lengths and diameters of the tubular structure representing the LVAC. Additionally, the CINE data was used to determine maximum necessary motion for each Cartesian direction of a stage. The results of these measurements are shown in Table 1 below:

Table 1: Minimum and maximum feature values for dimension and range of motion of the LVAC (in mm).

Feature	Min	Max
Diameter	6	10
Length	42	48
Motion X	0.36	1.36
Motion Y	0.16	1.12
Motion Z	0.7	1.43

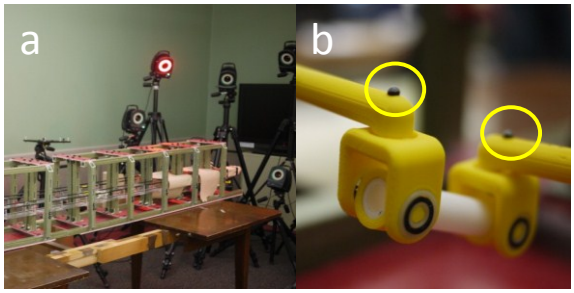

Fig. 6. a) Photograph of the phantom in the motion capture studio. b) Photograph of the end effector with fidicual markers installed.

B. *Design of Physical Prototype*

This phantom consists of two stages, one for each point of actuation of the LVAC representative tube structures. Each stage must account for three directions of motion: horizontal, vertical, and depth, or X, Y, and Z respectively. Each stage is designed as a long structure capable of rolling on a single fixed base. This rolling motion accounts for the Z direction of actuation. On top of this rolling Z plane rest two carts which are translated together using racks and pinion. These parallel carts implement the X direction of motion. Mounted to one of these carts is the motor for Y motion and built into the second cart is the Y rack and pinion. Carbon fiber driveshafts connect both X and Y motions to their respective motors. The end result of this stage configuration is a 2.5 m long semi-enclosed rectangular stage with an end-effector capable of movement in any of the three Cartesian directions.

From the MRI data collected it was determined that the maximum beating heart motion called for less than a 2 millimeter (mm) translation of the LVAC. However, for configurability, each stage was designed capable of a 20 mm range of motion. Since space inside an MRI scanner is limited, the phantom was designed to be as small as possible with the ability to complete its three Cartesian motions.

The resulting size of the phantom is around 30% larger than the dimensions proposed in [11] due to unforeseen constraints with building materials and fabrication facilities. However, the phantom still fits within the constraints of the MRI bore which is constrained to 60 cm horizontally and 40 cm vertically as described in [12]. The overall dimensions of the phantom inside the MRI scanner are 37 cm high and 23.5 cm wide. The robot should enter the phantom from the opposite side of the scanner. Each individual stage is less than 7 centimeters (cm) wide and 5 cm tall and the tank is only 14 cm tall leaving adequate space for a robotic manipulator to enter the phantom inside the MRI scanner. The base was designed to accommodate six stages rather than two so that two more tubular structures may be added in future work.

Preliminary Cartesian stages [11] were built using only carbon fiber in a truss configuration and transmitted power through carbon fiber driveshafts. However, issues were found with the straightness of the carbon fiber trusses. A better solution was to use laser-cut acrylic as the foundation

of the stages and carbon fiber rods across the top of the stage for rigidity. The proposed carbon fiber driveshafts provided too much torsional flexibility and were replaced by aluminum 7075 alloy rods. These aluminum driveshafts rotate through PTFE bushings. The remaining structural parts of the stage were constructed of ABS plastic or acrylic.

Fig. 7 contains selected photographs of the two stages and the base. Fig. 7(a) shows a top down view of the three motors from one stage installed into the base. Fig. 7(b) shows the end-effectors of the two stages linked to control opposing ends of the tube to represent the LVAC. Fig. 7(c) shows the fully assembled phantom in its entirety.

The base was designed of structural fiberglass. This material was the least flexible of the plastics and composites we tested (LDPE, PVC. Garrolite, Acrylic). The components are fastened together using plastic rivets where possible, and aluminum rivets in sections with limited space. Brass spur gears and racks were chosen because of the strength and availability. Though non-ferrous metal components were occasionally used in this design, the design has minimal use of metals within 2.5 m of the MRI's magnetic center.

C. MRI Compatibility

A critical concern to address was the possibility of MRI imaging artifacts being introduced by the electrically conductive brass and carbon fiber components which may generate eddy currents. To test the compatibility of the system, a single stage with two motors and all of its metal drive components installed was operated inside the MRI with a bottle of contrast agent as shown in Fig. 8(a).

No difference in SNR was observed on the bottle images between the conditions of no-phantom and phantom present but not actuated. Significant benefit was found from passing all cables through the waveguide as shown in Figs 8(b) and 8(c). Fig. 8(b) was collected with the unshielded motor and encoder cables passing through a wave guide from the control room, while Fig. 8(c) was collected with the unshielded cables passing through the door to the MR scanner room. The SNR while using the waveguide was calculated to be 90.9 ± 15.4 with the motors in operation,

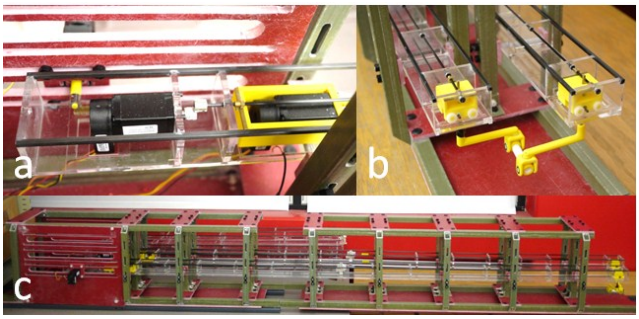

Fig. 7. Selected photographs of the two stages and the base. a) Top down view of the three motors from one stage installed into the base. b) End effectors of the two stages linked to control opposing ends of the tube to represent the LV. c) Fully assembled phantom.

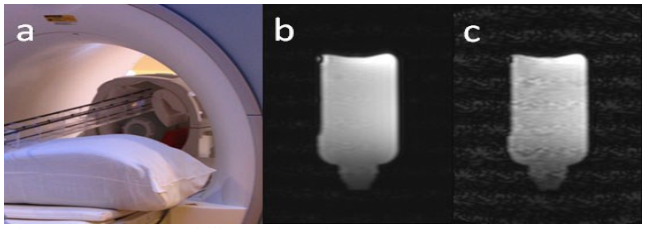

Fig. 8. MRI compatability testing of cartesian stage. a) Stage running in an MRI with contrast agent bottle. b) Resulting long-axis (Z direction) MRI image with cables through a wave guide. c) Resulting long-axis image without wave guide.

and a SNR of 89.4 ± 2.6 with the motors idling. It is hypothesized that the noise is largely a byproduct of the unshielded cables, which must enter the MR scanner room, acting as radiofrequency (RF) transmitters for the signals they carry. Currently, shielding options are under evaluation.

D. Motion Accuracy

After confirming the compatibilty with the MR scanner, the system controlled behavior needed evaluation. The movements tested by the motion capture system were all set to be 1.57 mm (100 steps of the motor with 10X microstepping) and the results are as follows: mean achieved motion was 1.24 ± 0.085 mm, yielding a total percent error of 21.1%. These measurements were obtained by filtering the data collected with the motion capture system at 120 hz using a running average. The absolute value difference between the steady state intial and final positions were then calculated for all trials. An example of these data can be seen in Fig. 9, which shows the desired position, and the data from the motion capture system, both filtered and unfiltered.

IV. Discussion

The design of the described phantom is the result of systematic analysis with the physicians of our group, and of the imaging and surgical needs associated with the particular clinical surgical paradigm. However, certain constraints arise from the decision to limit the mechatronics complexity of

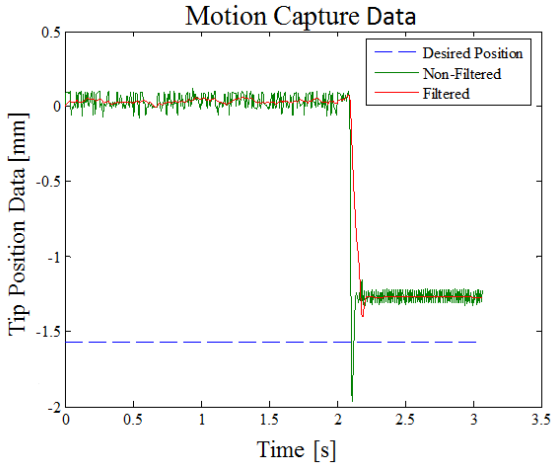

Fig. 9. Filtered (green) and unfiltered (red) position data from one motion capture trial

this device. One limitation of the phantom is that it does not replicate the fluid dynamic conditions inside the moving LVAC, or provide the effects of blood flow on a robotic manipulator. This is because the current design is particularly developed as a low-cost and simpler alternative to excised dynamic heart models. Another limitation of the design is that it currently does not replicate the changing diameter of the aorta. To eliminate the complexity of such mechanisms, we selected to construct the tubular structures that represent the LVAC with a diameter equal to the smallest diameter calculated from the MR CINE series. This limitation makes maneuvering through those structures far more challenging, thereby testing any robotic manipulator under extreme conditions.

In this proof-of-concept work, we simulated cardiac motion. Motion due to respiration was not present since breathhold CINE cardiac images were used to extract the mimicked motion waveforms. However, this does not limit the demonstration of phantom performance, since respiratory motion is much slower and of wider strokes than cardiac motion. Respiratory motion can be included if, for example, real-time free-breathing MRI is used to calculate the X, Y, and Z coordinates rather than CINE.

V. Conclusion

This work presents a dynamic phantom for mimicking the global motion of the LVAC. Using remote actuation and suitable materials, the phantom was proved MR compatible in a 1.5T scanner. Although it did have an impact on increasing the noise. this phantom did not introduce image distorting artifacts. This phantom serves as the first step and a platform for development for modeling the intracardiac landscape with actuated cylindrical passages.

VI. Future Work

This work will now be expanded to also model the trocar and LVAC in addition to the aortic annulus as well as evaulate methods for shielding to reduce RF noise.

Acknowledgment

The authors would like to thank Karen E. Chin, BS, RCS and Dipan J. Shah, M.D., FACC of the Methodist DeBakey Heart & Vascular Center for their invaluable time and use of their MRI scanner.

References

[1] L. H. Cohn, Future directions in cardiac surgery, Am Heart Hosp J, vol. 4, Summer 2006, pp. 174-8.

[2] M. M. Reijnen, et al., Future of operating rooms, Surg Technol Int, vol. 14, 2005, pp. 21-7.

[3] G. W. Taylor and D. G. Jayne, Robotic applications in abdominal surgery: their limitations and future developments, Int J Med Robot, vol. 3, Mar 2007, pp. 3-9.

[4] T. Boltz, et al., An anthropomorphic beating heart phantom for cardiac X-ray CT imaging evaluation, Journal of Applied Clinical Medical Physics, 2009, vol. 11.

[5] M. Li, et al., Robotic system for transapical aortic valve replacement with MRI guidance, Med Image Comput Comput Assist Interv, vol. 11, 2008, pp. 476-84.

[6] N. V. Tsekos, et al., Magnetic resonance-compatible robotic and mechatronics systems for image-guided interventions and rehabilitation: a review study, Annu Rev Biomed Eng, vol. 9, 2007, pp. 351-87.

[7] E. R. McVeigh, et al., Real-time interactive MRI-guided cardiac surgery: aortic valve replacement using a direct apical approach, Magn Reson Med, vol. 56, Nov 2006, pp. 958-64.

[8] E. Yeniaras, et al., A Novel Virtual Reality Environment for Preoperative Planning and Simulation of Image Guided Intracardiac Surgeries with Robotic Manipulators, Stud Health Technol Inform 163, 2011, pp. 716-722.

[9] E. Yeniaras, et al., Magnetic Resonance Based Control of a Robotic Manipulator for Interventions in the Beating Heart, Proceedings of 2011 IEEE International Conference on Robotics and Automation (ICRA 2011), Shanghai, China, 2011, pp.6270-6275..

[10] E. Yeniaras, et al., Towards A New Cyber-Physical System for MRI-Guided and Robot-Assisted Cardiac Procedures, in Proc. 10th Annu. IEEE International Conf. on Information Technology and Applications in Biomedicine (ITAB), Corfu, Greece, 2010, pp. 1-5.

[11] N. von Sternberg, et al., Design of an actuated phantom to mimic the motion of cardiac landmarks for the study of image-guided intracardiac interventions, in International Conference on Robotics and Biomimetics (ROBIO), Tianjin, China, 2010, pp. 856-861.

[12] N. V. Tsekos, et al., A general-purpose MR-compatible robotic system: implementation and image guidance for performing minimally invasive interventions, IEEE Eng Med Biol Mag, vol. 27, May-Jun 2008, pp. 51-8.

[13] A. Krieger, et al., Design of a novel MRI compatible manipulator for image guided prostate interventions, Biomedical Engineering, IEEE Transactions on, vol. 52, 2005, pp. 306-313.

[14] E. Christoforou, et al., Performance of interventions with manipulator-driven real-time MR guidance: implementation and initial in vitro tests, Magn Reson Imaging, vol. 25, Jan 2007, pp. 69-77.

[15] Z. Deng, et al., Perceptually Guided Expressive Facial Animation, in Proceedings of 2008 Simposium on Computer Animation (SCA'08).,Dublin, Ireland, 2008, pp. 67-76.